

Vortex Dynamics in Tubular Fluid Membranes

Udaya Maurya,¹ Surya Teja Gavva,² Arpan Saha,³ and Rickmoy Samanta⁴

¹*Institute for Plasma Research, Bhat, Gandhinagar, India*

²*Department of Computer Science, Rutgers University, Piscataway, NJ 08854-8019, USA*

³*IMECC UNICAMP, Campinas, São Paulo, Brazil*

⁴*Birla Institute of Technology and Science Pilani, Hyderabad 500078, India*

(Dated: February 19, 2025)

arXiv:2502.11206v2 [physics.flu-dyn] 18 Feb 2025

Abstract

Abstract: We construct 2D viscous flow sourced by a point vortex embedded in a thin tubular membrane, coupled to external embedding fluids. The cylinder topology enforces the creation of an additional saddle in the flow field, consistent with Poincaré Index Theorem. In this setup, the incompressibility of the membrane fluid can be utilized to cast the dynamics of a multi-vortex system in the form of a Hamiltonian on the cylinder, which depends on the fluid viscosities and vortex strengths. The cylinder geometry breaks the in-plane rotational symmetry of the membrane and leads to several interesting features in the multi-vortex dynamics, distinct from flat and spherical fluid membranes. For a two vortex system of same circulation, we observe closed orbits with the intervortex separation oscillating in time. The compact angular direction of the membrane tube also allows two distinct closed orbits instead of one, under suitable initial conditions. Vortex pairs (vortices with opposite circulation) move together along helical geodesics in accordance with a conjecture by Kimura Ref. [50], *Proceedings of the Royal Society A.455245–259 (1999)*. We also explore relative equilibria of multi-vortex systems in this setup and demonstrate vortex leapfrogging via numerical simulations. Our results will be interesting in the context of microfluidic flows arising in nature as well as experimental studies in membrane tubes similar to Ref. [17], *PNAS 108 (31) 12605-12610 (2011)*.

I. INTRODUCTION

The collective dynamics of biological nanomachines at fluid interfaces and membranes is currently an active arena for studying fascinating aspects of dynamical systems. These self-driven motors are capable of converting chemical or other forms of energy into mechanical motion. Moreover, mutual hydrodynamic interactions can often drive the system into an organized state. Biological membranes are particularly interesting in this context because of their fluidic nature [1], which is vital for many living processes. Such a membrane can be well approximated as a thin 2D sheet of viscous fluid with associated flows governed by low Reynolds hydrodynamics [2]. Moreover, the membrane fluid can exchange momentum with the external embedding fluids in the ambient space, thus they are essentially quasi-2D in nature. The early works of Saffman and Delbrück Ref. [3, 4] explored the low Reynolds hydrodynamics of inclusions embedded in such quasi-2D, flat membranes, followed by sev-

eral advancements Ref. [5–10, 12–14]. The quasi-2D nature of the membrane introduces an additional length scale (Saffman length) which is the ratio of the membrane viscosity (η_{2D}) and the viscosity of the external fluid (η). Beyond the Saffman length, the in-plane flows are governed by the traction stress from the external embedding fluids. In addition to this interesting feature, membranes found in nature typically have a confined geometry with non-zero curvature. Moreover, they host a large number of inclusions. The impact of membrane topology and curvature on dynamics of such inclusions has been studied in many recent works, Ref. [11, 15–30] and also being probed in recent experiments, Ref. [15, 17, 19]. In particular, good agreement with Saffman Delbrück theory has been demonstrated in membrane tubes Ref. [17].

The physics of rotating motors in fluid interfaces has recently been the subject of many theoretical and experimental investigations, Ref. [31–43]. In this paper, we focus on the hydrodynamic interactions of rotating inclusions embedded in tubular fluid membranes. The inclusions considered in this work may be considered as driven-to-rotate entities which induce vortex-like flows in membranes. Such vortices are known to self-organize into crystallized states under suitable conditions and exhibit hyperuniform order [44–47] in flat membranes. The dynamics of such rotating units in spherical fluid membranes is being explored as well, see Ref. [26]. The tubular membrane geometry that we explore in this paper is distinct from flat and spherical membranes, since the in-plane rotational symmetry is broken. We find that this breakdown of rotational symmetry, along with the confined cylinder topology (in the angular direction) leads to several interesting features in the dynamics of microvortex assemblies in membrane tubes. First, we show that the cylinder topology enforces the creation of an additional saddle defect in the flow sourced by a single vortex, consistent with Poincaré Index theorem. Next, utilizing the incompressibility condition of the membrane fluid flow, we cast the dynamics of the multi-vortex system in terms of a Hamiltonian on the cylinder, similar to the approach followed in flat membranes [46–48]. The Hamiltonian depends on the system parameters, the Saffman length λ , the tube radius R and the circulation strength of the vortices. This offers experimentally accessible tuning parameters to control the dynamics of the multi-vortex system. Focusing on a simple system of two vortices of same circulation strength τ , we show that the breaking of rotational symmetry leads to non-conservation of the inter-vortex separation, unlike flat and spherical

fluid membranes. The vortices generically move in closed orbits, which can be severely distorted by tuning the initial inter-vortex separation as well as the parameter $\frac{\lambda}{R}$. For example, upon reducing the value of $\frac{\lambda}{R}$ we find that the single orbit breaks into two smaller orbits. Also, when they are initially sufficiently separated along the longitudinal (z-axis) direction of the tube, we observe that the vortices prefer two distinct orbits that cover the entire circumference of the tube. Two vortices with opposite circulation generically move together along helical trajectories, in accordance with a conjecture by Kimura [50]. We also explore relative equilibria and relative periodic orbits including vortex leapfrogging. Besides being of experimental relevance Ref. [17], we believe our results will be interesting for understanding the possibility of formation of vortex crystals and exploring emergent hyperuniformity in cylindrical surfaces. Moreover, many of our results will be applicable to more general setups involving rotating motors (both living and non-living) in tubular fluid interfaces.

The paper is organized as follows: In Sec. II we provide a brief review of hydrodynamics of generic curved membranes, following [16] and [26, 28, 29]. Specializing to membrane tubes, we construct the point vortex solution, explore topological aspects of the flow and provide the multi-vortex Hamiltonian in Sec. III. The dynamics governed by the Hamiltonian is next explored in Sec. IV, initially focusing on two vortices and then extending to multi-vortex systems, illustrating the conserved quantities. Investigations on vortex equilibria, relative periodic orbits and vortex leapfrogging in the tubular geometry are also provided. We finally conclude with a future outlook in Sec. V.

II. MEMBRANE HYDRODYNAMICS

In this section, we present a brief review of viscous hydrodynamics in membranes of fixed geometries, closely following Ref. [16] and Ref.[26, 28]. We will describe the setup for arbitrarily curved but fixed membrane geometry and later specialize to cylindrical membranes. In the fluid approximation, the membrane is considered as a two-dimensional, curved, incompressible monolayer of viscosity η_{2d} surrounded by external embedding fluids of different viscosities, both outside and inside the membrane. In order to simplify the analysis, we consider situations where the membrane geometry is fixed in time and only consider in-plane

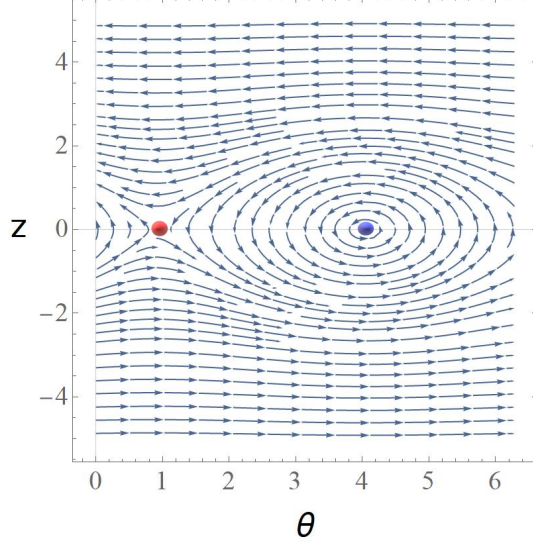


FIG. 1: Plot of the vortex solution Eq. (8) with the blue and red dot representing the vortex core and saddle respectively.

shear flows with no normal component. The membrane fluid is coupled to the external embedding fluids, and hence the membrane is essentially quasi 2D. The key hydrodynamic equations appropriate for this setup are as follows:

$$D^\alpha v_\alpha = 0 \quad (1)$$

$$\sigma_\alpha^{ext} = \underbrace{-\eta_{2D} (K(\vec{x}) v_\alpha + D^\mu D_\mu v_\alpha)}_{\text{Membrane stress}} + \underbrace{D_\alpha p}_{\text{External stress}} + T_\alpha \quad (2)$$

$$\nabla \cdot \mathbf{v}_\pm = 0, \quad \eta_\pm \nabla^2 \mathbf{v}_\pm = \nabla_\pm p^\pm \quad (3)$$

$$T_\alpha = \sigma_{\alpha r}^-|_{r=R} - \sigma_{\alpha r}^+|_{r=R}, \quad \sigma_{ij}^\pm = \eta_\pm (D_i v_j^\pm + D_j v_i^\pm) - g_{ij} p_\pm \quad (4)$$

$$\mathbf{v}_\pm|_{r=R} = v. \quad (5)$$

In the above equations, we use Greek indices to represent the in-plane 2D membrane coordinates. Latin indices are used for 3D coordinates to describe flows in the ambient 3D embedding fluids surrounding the 2D membrane. Eq. (1) is the incompressibility condition for the 2D membrane fluid velocity field v_α . D is the metric compatible covariant derivative. Eq. (2) is the boundary condition for tangential stress balance at the membrane surface. σ_α^{ext} represents the local stress exerted by the rotating inclusions embedded in the membrane (this will be a point torque for the following discussions) and is balanced by the in-plane membrane stress and the tangential traction stress from the external embedding fluids (denoted by T_α) in the equation. Generic membrane surface coordinates are denoted by “x”. Notably,

in the low Reynolds regime, inertia terms are absent and fluid flows are dictated by Stokes equations, with viscosity η_{2D} being the viscosity of the membrane fluid. $K(\vec{x})$ is the local Gaussian curvature and p represents the 2D membrane pressure. The membrane fluid is surrounded by external 3D embedding fluids with viscosities η_{\pm} and pressure p_{\pm} where “ \pm ” denotes the outer/inner fluid respectively. Eq. (3) are the relevant Stokes equations for the external incompressible embedding fluids in 3D. Eq. (4) gives the expression for the traction vector T_{α} . The coordinate r represents a generic coordinate along the membrane normal. Finally, Eq. (5) is the no-slip boundary condition. We also define two Saffman length scales

$$\lambda_+ = \frac{\eta_{2D}}{\eta_+}, \quad \lambda_- = \frac{\eta_{2D}}{\eta_-}.$$

In what follows, we will choose $\eta \equiv \eta_+ = \eta_-$ and thus restrict to a unique Saffman length $\lambda \equiv \frac{\eta_{2D}}{\eta}$. Higher values of $\frac{\lambda}{R}$ indicate the high curvature regime (thin membrane tube).

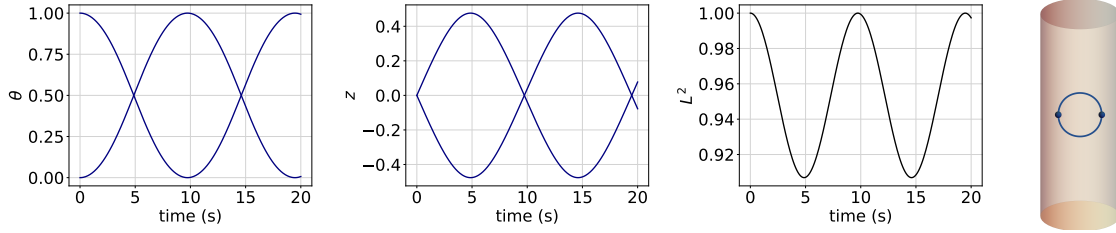
III. VORTEX SOLUTION AND MULTI-VORTEX HAMILTONIAN

In this section, we specialize to membranes of cylindrical geometry which have zero Gaussian curvature ie. $K(x) = 0$ in Eq. (2). This greatly simplifies the coupled system of equations and one can arrive at an analytic vortex solution in this setup. Note that even in the absence of Gaussian curvature, the extrinsic geometry of the cylinder modifies the momentum exchange between the membrane fluid and the external embedding fluids and has significant impact on the multi-vortex dynamics we are going to study. We refer to Appendix Sec. A for a detailed computation of the single vortex solution and here summarize the key results. The incompressible nature of the membrane fluid can be utilized to express the membrane velocity field confined to the cylinder surface in terms of a scalar stream function ψ as follows (here θ and z are the usual angular and axial coordinates along the cylinder surface of fixed radius R):

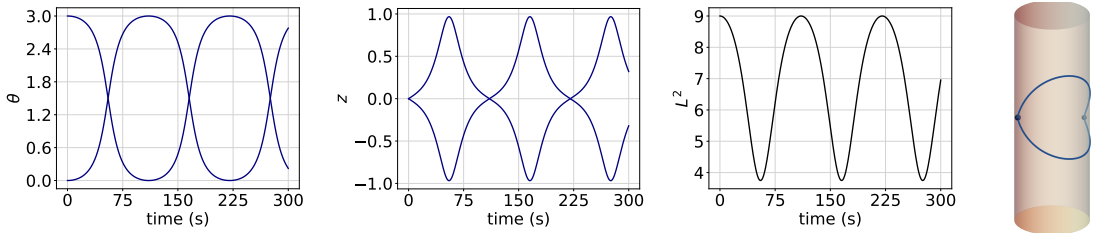
$$v_{\theta} = \partial_z \psi \quad v_z = -\frac{1}{R} \partial_{\theta} \psi \quad (6)$$

As shown in detail in Appendix Sec. A, in the limit of thin tubular membranes, the stream function ψ for a point vortex situated at the origin $(\theta, z) = (0, 0)$ takes the following simple form

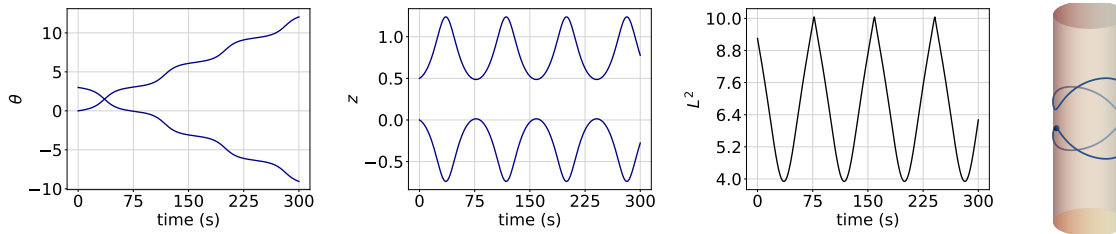
$$\psi(\theta, z) = \frac{\tau}{4\pi\eta_{2D}} \left(-\log \left[1 - 2e^{-\frac{|z|}{R}} \cos \theta + e^{-\frac{2|z|}{R}} \right] + \sqrt{\frac{\lambda}{2R}} e^{-\frac{\sqrt{2}|z|}{\sqrt{\lambda R}}} \right). \quad (7)$$



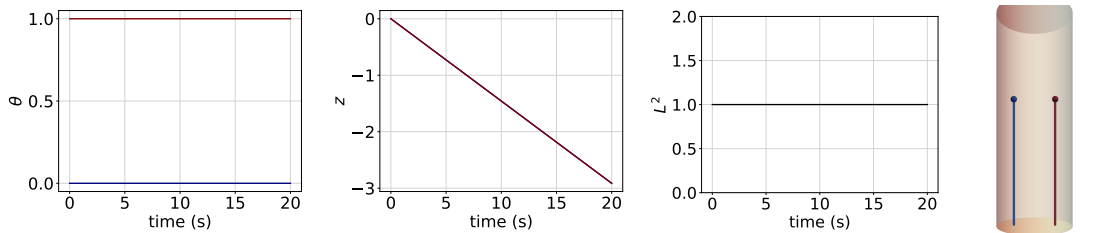
(a) Case A



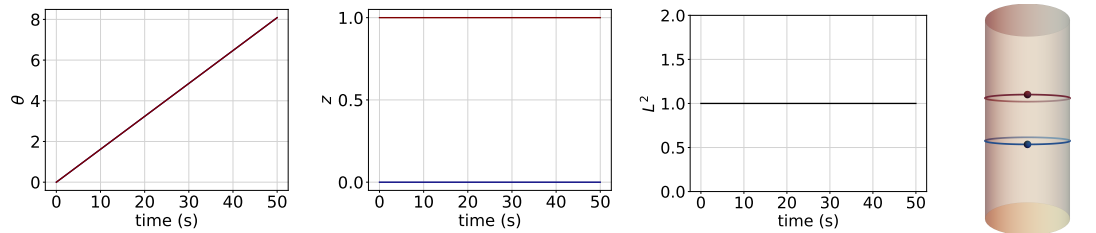
(b) Case B



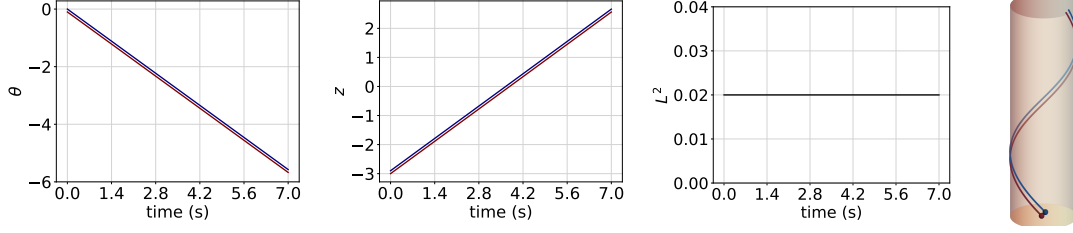
(c) Case C



(d) Case D

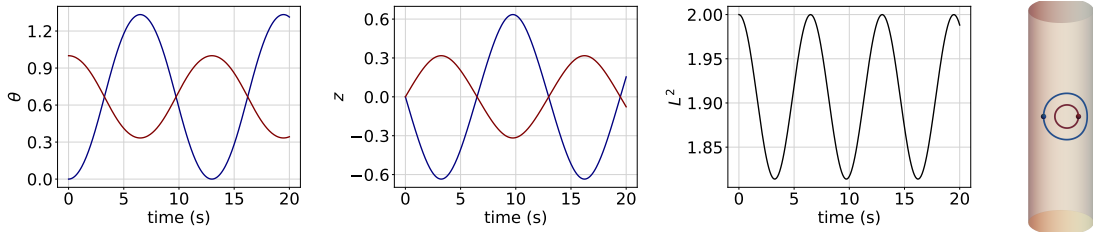


(e) Case E

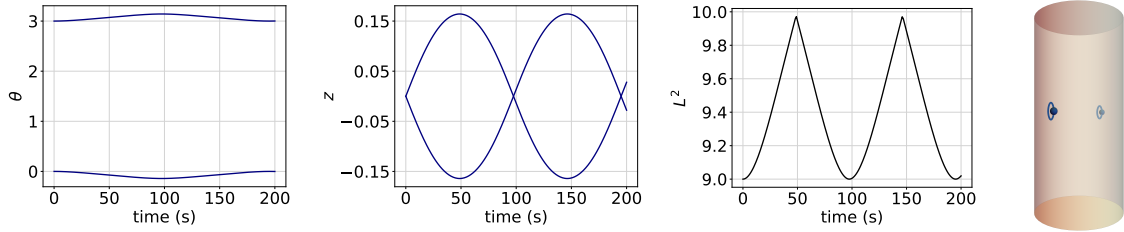


(f) Case F

FIG. 2: Two vortex dynamics in the membrane tube with $\frac{\lambda}{R} = 100$. We show variations in vortex locations (θ, z) and the evolution of L^2 defines in Eq. (13) wrt time. For the 3D cylinder plot appearing on the extreme right, blue dots indicate initial location of vortices with positive circulation, while red dots indicate vortices with negative circulation. The same color code is used for the vortex trajectories.



(a) Same configuration as Fig. (2a) but with unequal vortex strengths of same sign.



(b) Same configuration as Fig. (2b) but with $\frac{\lambda}{R} = 5$

FIG. 3: Vortex dynamics with tuning of parameters

where τ is the strength of the circulation. Thus, for a vortex located at (θ_0, z_0) on the membrane tube, the velocity field at any location (θ, z) is given by

$$\begin{aligned}
 v_\theta[\theta, z, \theta_0, z_0] &= \frac{\tau(z-z_0)}{4\pi R \eta_{2D} |z-z_0|} \left(\frac{2-2\cos(\theta-\theta_0)}{1+e^{\frac{2|z-z_0|}{R}} - 2\cos(\theta-\theta_0)} e^{\frac{|z-z_0|}{R}} - e^{-\sqrt{\frac{2}{R\lambda}}|z-z_0|} \right) \\
 v_z[\theta, z, \theta_0, z_0] &= -\frac{\tau}{4\pi\eta_{2D} R} \frac{\sin(\theta-\theta_0)}{\cos(\theta-\theta_0) - \cosh \frac{z-z_0}{R}}
 \end{aligned} \tag{8}$$

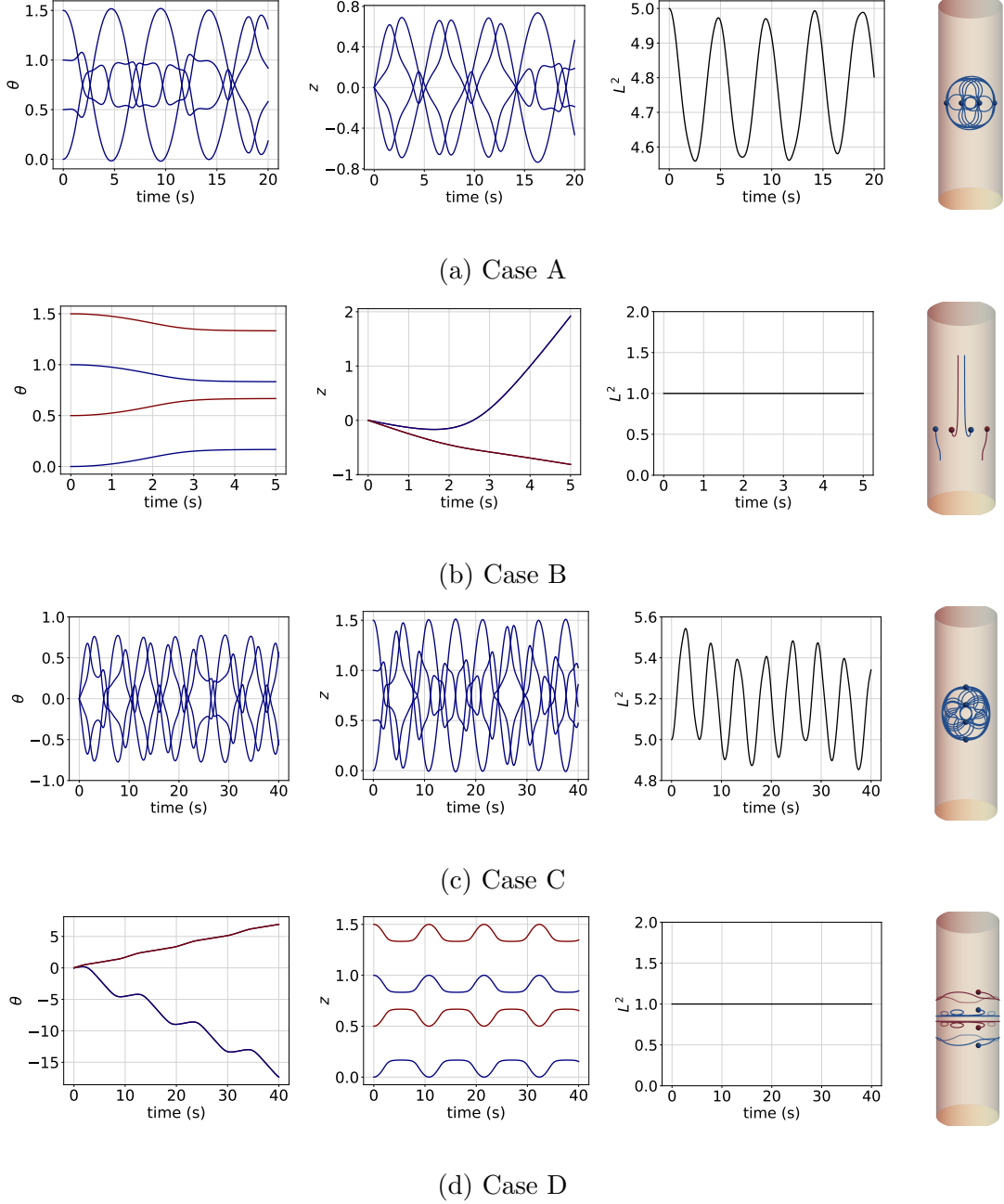


FIG. 4: Multi-vortex dynamics in the membrane tube

The vortex solution is presented in Fig. 1. As evident from the streamlines, the cylinder topology enforces the creation of an additional saddle defect in the flow such that the net index is zero, consistent with Poincaré Index theorem. We now cast the dynamics of the multi-vortex system such that a vortex is simply advected by the local fluid flow generated by the remaining vortices. Following standard treatment in vortex literature, such dynamics of the many-vortex system can be encapsulated in the form of a Hamiltonian on the cylinder,

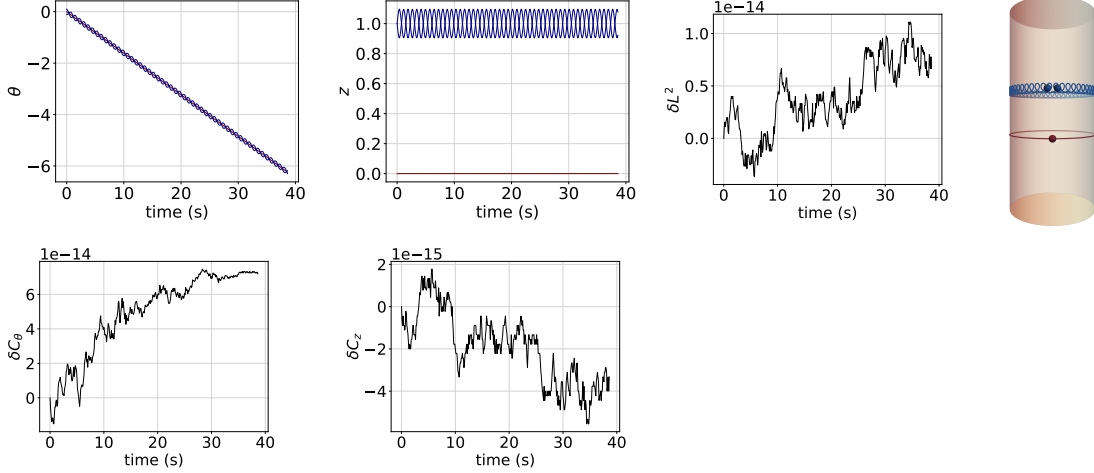


FIG. 5: Vortex leapfrogging for $\frac{\lambda}{R} = 100$ in a 3 vortex system. The vortex with positive circulation $\tau = +1$ is marked red, while two vortices of circulation $\tau = -\frac{1}{2}$ each is shown in blue, with the same color code for trajectories. Numerical errors in L^2, C_θ, C_z are also shown.

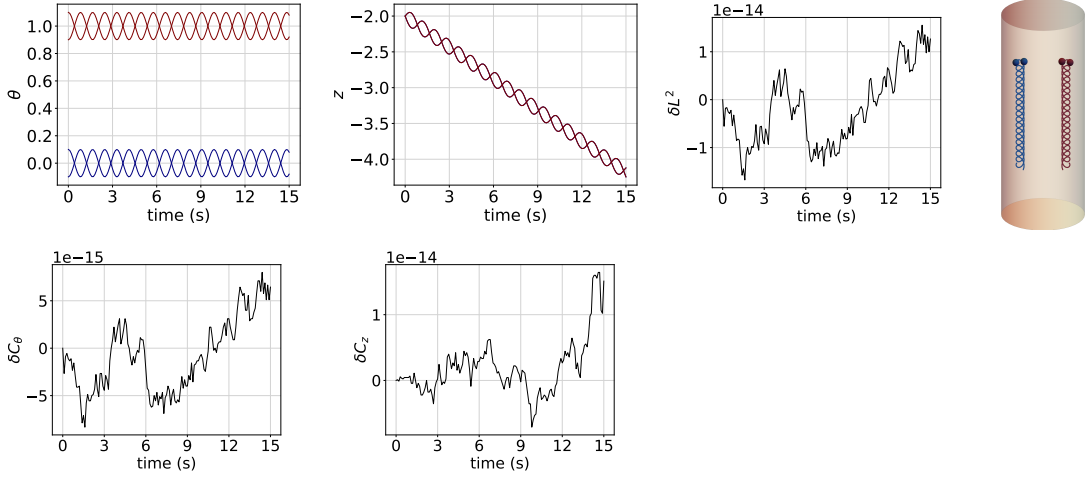


FIG. 6: Vortex leapfrogging for $\frac{\lambda}{R} = 100$ in a 4 vortex system. Two vortices with positive circulation $\tau = +1/2$ each are marked red, while two vortices of circulation $\tau = -\frac{1}{2}$ each are shown in blue, with the same color code for trajectories. Numerical errors in L^2, C_θ, C_z are also shown.

utilizing the cylinder stream function Eq. (7)

$$H = \sum_{i \neq j} \frac{\tau_i \tau_j}{4\pi\eta_{2D}} \left(-\log \left[1 - 2e^{-\frac{|z_i - z_j|}{R}} \cos(\theta_i - \theta_j) + e^{-\frac{2|z_i - z_j|}{R}} \right] + \sqrt{\frac{\lambda}{2R}} e^{-\frac{\sqrt{2}|z_i - z_j|}{\sqrt{\lambda R}}} \right) \quad (9)$$

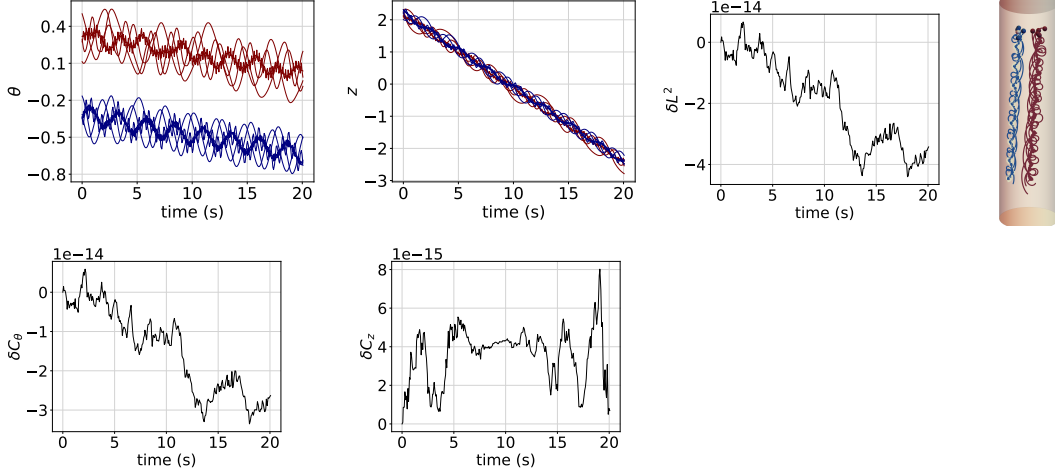


FIG. 7: Vortex leapfrogging for $\frac{\lambda}{R} = 100$ in a 10 vortex system. Five vortices with random splittings of vortex strengths adding up to a net positive circulation $\sum_i \tau_i = +1$ are marked red, while remain vortices with random splittings of vortex strengths adding up to a net negative circulation $\sum_i \tau_i = -1$ are shown in blue, with the same color code for trajectories. Numerical errors in L^2, C_θ, C_z are also shown.



FIG. 8: Left: An equilibria of 4 vortices arranged in a ring, with intervortex separation $\frac{\pi R}{2}$, Right: Mild perturbation in one of the vortex location in the ring renders the system unstable.

where $Q_i = \sqrt{|\tau_i|}R \theta_i$ and its associated conjugate momentum is $P_i = \sqrt{|\tau_i|}z_i$, in terms of which the dynamics is governed by the usual Hamilton's equations $\dot{Q}_i = \partial_{P_i}H$, $\dot{P}_i = -\partial_{Q_i}H$. In the usual coordinates (θ, z) , the dynamical equations for the multi-vortex system thus reads

$$\begin{aligned}
 R \dot{\theta}_i &= \sum_{j \neq i}^N v_\theta[\theta_i, z_i, \theta_j, z_j] \\
 \dot{z}_i &= \sum_{j \neq i}^N v_z[\theta_i, z_i, \theta_j, z_j]
 \end{aligned}
 \tag{10}$$

where the velocity field (v_θ, v_z) is given by Eq. (8). Written explicitly, the dynamical equations take the following form

$$R\dot{\theta}_i = \sum_{j \neq i}^N \frac{\tau_j(z_i - z_j)}{4\pi R \eta_{2D} |z_i - z_j|} \left(\frac{2 - 2\cos(\theta_i - \theta_j) e^{\frac{|z_i - z_j|}{R}}}{1 + e^{\frac{2|z_i - z_j|}{R}} - 2\cos(\theta_i - \theta_j) e^{\frac{|z_i - z_j|}{R}}} - e^{-\sqrt{\frac{2}{R\lambda}} |z_i - z_j|} \right)$$

$$\dot{z}_i = - \sum_{j \neq i}^N \frac{\tau_j}{4\pi\eta_{2D}R} \frac{\sin(\theta_i - \theta_j)}{\cos(\theta_i - \theta_j) - \cosh \frac{z_i - z_j}{R}}. \quad (11)$$

The translational symmetry of the Hamiltonian leads to the conservation of the following quantities

$$C_\theta \equiv \sum_i \tau_i \theta_i \quad C_z = \sum_i \tau_i z_i \quad (12)$$

which is ensured in our multi-vortex simulations to a good accuracy (Numerical errors of the order of 10^{-14}). We further define a quantity

$$L^2 \equiv \frac{1}{2} \left| \sum_{i \neq j} \tau_i \tau_j l_{ij}^2 \right| \quad (13)$$

where $l_{ij}^2 = R^2 \text{Min}(\theta_i - \theta_j, 2\pi - (\theta_i - \theta_j))^2 + (z_i - z_j)^2$ is the distance function appropriate for the cylinder geometry. For the two vortex systems, we will denote the quantity in Eq. (13) by L_{12}^2 and reserve the notation L^2 for multi-vortex systems. The quantity L^2 is conserved in flat and spherical membranes but violated in membrane tubes due to loss of in-plane rotational symmetry, as will be explicitly demonstrated in the simulations presented in Sec. IV.

IV. VORTEX DYNAMICS IN MEMBRANE TUBES

In this section, we numerically simulate the vortex dynamics on the surface of the membrane tube using the dynamical equations Eq. (10). In all cases, we include a 3D plot showing the vortex trajectories on the surface of the membrane tube. Trajectories of vortices with positive circulation (anti-clockwise) are colored blue, while vortices of negative circulation (clockwise) are colored red. The initial locations of vortices are marked by a colored dot, following the same color code as the trajectories. We first discuss the two vortex case for $\frac{\lambda}{R} = 100$ in Figs. (2a-2f) for equal (or opposite) vortex strength. This typically results in closed orbits for vortex pairs of same circulation and helical geodesics for vortex pairs of opposite circulation. Next, in Fig. (3a) we show the trajectories for two vortices of

unequal strength but same sign, giving rise to concentric circular orbits. Fig. (3b) illustrates interesting effects resulting from tuning $\frac{\lambda}{R}$. Multi-vortex systems are explored in Figs. (4a-4d). Vortex leapfrogging and relative periodic orbits are illustrated in various situations Fig. (5-7) along with the associated numerical errors in conservation of C_θ and C_z . Finally, we study the stability of vortex rings in Fig. (8).

A. The two-vortex system

We first consider a two-vortex system of the same strength τ with $\lambda/R = 100$. In Fig. (2a), we show the variation of vortex locations (θ, z) and L_{12}^2 defined in Eq.(13) with time and the rightmost plot shows a trace of the vortex trajectories. From the plots, it is clear that a two vortex system which is initially closely spaced will orbit each other in a closed orbit, with the inter-vortex distance oscillating in time. This is in contrast to flat and spherical fluid membranes, where L_{12}^2 is conserved and arises due to the breaking of in-plane rotational symmetry in tubular membranes. However, the orbit shape gets remarkably distorted for vortices, which are initially well separated. This is illustrated in Fig. (2b) where the vortices are initially well separated along the angular $\hat{\theta}$ direction. This can also lead to pinching of a single closed orbit into two separate orbits. For example, two vortices initially well separated along the longitudinal \hat{z} direction of the tube prefer to go in separate orbits, encircling the tube, see Fig. (2c).

Comments on pinching of orbits: A mathematical understanding of these results emerges easily from the associated conserved quantities Eq. (12) and the conservation of the Hamiltonian Eq. (9). Using Eq. (12) one can eliminate say (θ_2, z_2) in favor of (θ_1, z_1) , thus the Hamiltonian constraint Eq. (9) becomes a function of only one of the vortex coordinates ie (θ_1, z_1) and the constants of motion ie. C_θ, C_z . Analyzing the level curves of this Hamiltonian in the $\theta_1 - z_1$ plane, one readily observes that for the situations described in Fig. 2a and Fig. 2b the contour plots are closed loops, while for Fig. 2c, they traverse the entire angular direction of the cylinder, see Fig. 9 of Appendix B for the relevant contour plots.

For the two-vortex system of opposite strength (also known as vortex pair), we observe vastly different interactions, see Fig. (2d-2f). A vortex pair separated along the angular (transverse) direction of the tube move in vertical parallel trajectories (Fig. 2d) while vortex pairs separated along the longitudinal direction of the tube move together along the transverse direction in separate closed orbits (Fig. 2e). Arbitrarily situated vortex pairs move together along helical geodesics, in accordance with a conjecture by Kimura Ref. [50]. Note that in all the situations with vortex pairs, the net circulation is zero and L^2 is conserved in time. These results are evident from Eq. (11) where for equal and opposite strength $\tau_1 = -\tau_2$ we find that $\dot{\theta}_1 = \dot{\theta}_2$ and $\dot{z}_1 = \dot{z}_2$. Using this fact, it is straightforward to compute the pitch of the helix z_P as presented in Eq. (B1) of Appendix B,

$$z_P = \frac{\frac{2\pi R \sin(\theta_1^i - \theta_2^i)}{\cos(\theta_1^i - \theta_2^i) - \cosh \frac{z_1^i - z_2^i}{R}}}{\frac{2 - 2 \cos(\theta_1^i - \theta_2^i) e^{\frac{|z_1^i - z_2^i|}{R}}}{1 + e^{\frac{2|z_1^i - z_2^i|}{R}} - 2 \cos(\theta_1^i - \theta_2^i) e^{\frac{|z_1^i - z_2^i|}{R}}} - e^{-\sqrt{\frac{2}{R\lambda}} |z_1^i - z_2^i|}} \quad (14)$$

where (θ_1^i, z_1^i) and (θ_2^i, z_2^i) are the initial locations of the vortex pair. Additionally, we note that the ratio of the vortex strengths τ_1/τ_2 and λ/R provide additional tuning parameters which can be used to control the vortex trajectories, as illustrated in Fig. (3a) and Fig. (3b) respectively. Fig. (3a) shows two concentric orbits arising from unequal vortex strengths, whereas in Fig. (3b) we simulate the same initial configuration as Fig. (2b) but with $\lambda/R = 5$. In this situation, the single closed orbit of Fig. (2b) breaks into two separate local closed orbits, as seen in Fig. (3b). This pinching can also be similarly understood in terms of the level sets of the Hamiltonian.

Comments on confined and unconfined dynamics of vortices: The confined dynamics of vortices of same circulation (or equivalently, the unconfined dynamics of vortices of opposite circulation) can be easily understood from the conservation of the vortex Hamiltonian Eq. 9 and the conservation of C_z , Eq. 12. For vortices of same circulation $\tau_1 = \tau_2 \equiv \tau$, $z_1 = \frac{C_z}{\tau} - z_2$ which implies $|z_1 - z_2| = \left| \frac{C_z}{\tau} - 2z_2 \right|$. Thus, the Hamiltonian decays exponentially as $z_2 \rightarrow \infty$, which is forbidden by energy conservation. This in turn explains the bounded orbits for vortices of same strength. On the other hand, for vortices of equal and opposite strength, then $|z_1 - z_2| = \left| \frac{C_z}{\tau} \right|$ which is a constant. Thus, the Hamiltonian conservation allows the vortices to drift together to large z leading to unconfined dynamics

in this situation.

B. Essential features of the multi-vortex system

Moving on to multi-vortex assemblies Fig. (4a-4d), we first simulate a set of 4 vortices arranged along the transverse ($\hat{\theta}$) direction of the membrane tube, of same (Fig. 4a) and alternating (Fig. 4b) circulations. All simulations are performed with $\lambda/R = 100$. A distinct feature of multi-vortex assemblies of the same strength (Fig. 4a) is that their dynamics remains confined in a region determined by the initial distribution, with L^2 oscillating in time. This can be again explained from the conservation of the Hamiltonian Eq. 9 like the two vortex system. On the other hand, the multi-vortex systems of alternating circulation (with zero net circulation) show unconfined dynamics, yet L^2 remains conserved in time, see Fig. 4b. Vortices initially situated along the longitudinal direction of the cylinder Fig. (4c) and Fig. (4d) share the same features as their transverse counterparts, ie. Fig. (4a) and Fig. (4b), except the fact that the compact cylinder topology enforces the vortices of alternating circulations to exhibit closed orbits wrapping the entire membrane tube, see Fig. (4d). In Fig. (5-7) we demonstrate the interesting phenomenon of vortex leapfrogging in the tubular fluid membrane. In such situations, the vortices move in periodic or quasi-periodic orbits along with translation along the tube surface. They are fairly easy to design using the results from two vortex systems. As observed in Fig. (2d-2f), vortex pairs (of opposite circulation) translate together while vortices of same circulation perform periodic orbits with no net translation. In order to achieve relative periodic orbits (leapfrogging), one can take a vortex pair (of circulation $\tau_1 = +1$ and $\tau_2 = -1$) and divide them into two groups A and B, such that the circulations in group A add up to +1 while that of Group B add up to -1 (this is also known as “Vortex splitting”). The vortices in Group A and Group B will translate together, while within each individual group we will have periodic or quasi periodic orbits of the split vortices. This is illustrated in several leapfrogging scenarios in Fig. (5-7). Finally, we note that equilibria of vortex rings can be constructed for N vortices arranged along the transverse direction of the tube with intervortex separation $\frac{2\pi R}{N}$. This configuration is unstable and is illustrated in Fig. (8) for $N = 4$.

V. CONCLUSION

In this paper, we focus on the hydrodynamic interactions of vortex assemblies embedded in tubular fluid membranes. The tubular membrane geometry is distinct from flat and spherical membranes, due to loss of in-plane rotational symmetry. We find that the confined cylinder topology (in the angular direction) leads to several interesting features in the dynamics of microvortex assemblies in membrane tubes. We first construct an analytic vortex solution in this tubular fluid membrane setup and show that the cylinder topology enforces the creation of an additional saddle defect in the flow, consistent with Poincaré Index theorem. Next, the incompressibility condition of the membrane fluid flow is utilized to construct a Hamiltonian on the cylinder that governs the dynamics of the multi-vortex system. The Hamiltonian depends on the system parameters, the Saffman length λ , the tube radius R and the circulation strength τ of the vortices. This offers experimentally accessible tuning parameters to control the dynamics of the multi-vortex system. Focusing on a simple system of two vortices of same circulation strength τ , we show that the breaking of rotational symmetry leads to non-conservation of the inter-vortex separation, unlike flat and spherical fluid membranes. The vortices generically move in closed orbits, which can be severely distorted by tuning the initial inter-vortex separation as well as the parameter $\frac{\lambda}{R}$. In particular, we observe several situations where a single closed orbit breaks into two upon tuning system parameters. We also illustrate this pinching from a mathematical point of view by considering the level sets of the associated vortex Hamiltonian. Two vortices with opposite circulation generically move together along helical trajectories, thus confirming a conjecture by Kimura on the dynamics of vortex pairs Ref. [50]. We also explore relative periodic orbits and relative equilibria including vortex leapfrogging. Besides being of experimental relevance (Ref. [17]), we believe our results will be useful in the investigation of the possibility of formation of vortex (rotor) crystals and emergent hyperuniformity in cylindrical surfaces, analogous to the studies in flat membranes Ref. [44–47] and vortex simulations in superconductors, Ref. [49]. Moreover, dynamics of rotating matter in fluid interfaces is currently an active area of research Ref.[31–43], both from an experimental and theoretical perspective. We believe many of our results will be applicable to more general setups involving rotating motors (both living and non-living) in tubular fluid interfaces. It will also be interesting to connect our results to vortex and mass dynamics in inviscid cylinder

geometries, Ref.[51, 52]. An analysis of thermal fluctuations in this setup, along the lines of the work of Sokolov and Diamant Ref. [53] is left for the future.

VI. ACKNOWLEDGMENTS

We are very thankful to Naomi Oppenheimer, Haim Diamant, Mark Henle, Sarthak Bagaria, Samyak Jain, Prasad Perlekar and Mustansir Barma. R.S is supported by DST INSPIRE Faculty fellowship, India (Grant No.IFA19-PH231), NFSG and OPERA Research Grant from Birla Institute of Technology and Science, Pilani (Hyderabad Campus). The work is dedicated to the memory of Professor Alex J. Levine, UCLA.

Appendix A: Construction of the Vortex solution in the Tubular Fluid Membrane

In this Appendix, we will sketch the construction of the flow sourced by a point vortex embedded in a tubular fluid membrane, extending Ref.[16, 26, 28]. We will first provide the vortex solution for cylindrical fluid membranes of arbitrary radius and finally consider the limit of thin tubular membrane, which is of relevance to our study in this paper. The cylinder surface metric in the usual (θ, z) coordinates is

$$ds^2 = R^2 d\theta^2 + dz^2 \tag{A1}$$

and

$$\epsilon_{\alpha\beta} = \begin{pmatrix} 0 & R \\ -R & 0 \end{pmatrix} \tag{A2}$$

is the corresponding Levi Civita tensor. The incompressibility condition of the membrane fluid (Eq.(1) of main text) allows us to write the 2D velocity field on the cylinder surface in terms of a scalar stream function ψ as follows:

$$v_\alpha = \epsilon_{\alpha\beta} D^\beta \psi.$$

Decomposing ψ in terms of eigenmodes of the Laplace Beltrami operator for the cylinder surface, we get

$$v_\alpha = \epsilon_{\alpha\beta} D^\beta \left(\int d\Lambda A(\Lambda) e^{i\Lambda_\mu x^\mu} \right) \tag{A3}$$

where $\Lambda_\alpha \equiv (n, q \equiv \frac{k}{R})$ and $x^\alpha \equiv (\theta, z)$ such that $\Lambda_\mu x^\mu = n\theta + \frac{k}{R}z$. The unknown coefficients $A(\Lambda)$ will be solved below using the stress-balance condition Eq.(2) of main text. In the stress balance condition, we insert the external point torque $\sigma_\alpha^{ext} = \tau \epsilon_{\alpha\gamma} D^\gamma \delta^2(\theta - \theta_0, z - z_0)$ and also take an anti-symmetric derivative on both sides of the equation to eliminate the membrane pressure p . The expression for the traction vector T_α appearing on the RHS of the stress balance condition in Eq.(2) requires a straightforward but somewhat long computation, which we just summarize below.

Computation of T_α : In order to compute the in-plane components of the traction vector T_α we utilize the known solution for Stokes flow in 3D (Eq.(3) of main text) in cylindrical coordinates following Happel and Brenner Ref.[54]:

$$\begin{aligned}\vec{v}^\pm(r, \theta, z) &= \vec{\nabla} f^\pm(r, \theta, z) + \vec{\nabla} \times [g^\pm(r, \theta, z)\hat{z}] + r\partial_r \left[\vec{\nabla} h^\pm(r, \theta, z) \right] + \partial_z h^\pm(r, \theta, z)\hat{z}, \\ p^\pm(r, \theta, z) &= -2\eta_\pm \partial_z^2 h^\pm(r, \theta, z),\end{aligned}$$

where f^\pm, g^\pm, h^\pm are harmonic functions of Laplacian operator in 3D in cylindrical coordinates. Such harmonic functions on the cylinder admit a decomposition

$$f^\pm(r, \theta, z) = \sum_{n=-\infty}^{\infty} \int_{-\infty}^{\infty} dq e^{i\Lambda_\mu x^\mu} F^\pm(\Lambda) \xi_n^\pm(qr)$$

and likewise for g^\pm, h^\pm . In the above expression,

$$\xi_n^+(qr) \equiv K_n(|q|r), \quad \xi_n^-(qr) \equiv I_n(|q|r)$$

where K_n and I_n are modified Bessel functions of order n of first and second kind respectively. The covariant components of the external fluid velocities thus read as follows:

$$\begin{aligned}v_r^\pm(\Lambda, r) &= |q|\tilde{\xi}_n^\pm(qr)F^\pm(\Lambda) + \frac{in}{r}\xi_n^\pm(qr)G^\pm(\Lambda) + H^\pm(\Lambda) \left[-|q|\tilde{\xi}_n^\pm(qr) + r \left(q^2 + \frac{n^2}{r^2} \right) \xi_n^\pm(qr) \right] \\ v_\theta^\pm(\Lambda, r) &= im\xi_n^\pm(qr)F^\pm(\Lambda) - |q|r\tilde{\xi}_n^\pm(qr)G^\pm(\Lambda) + inH^\pm(\Lambda) \left[|q|r\tilde{\xi}_n^\pm(qr) - \xi_n^\pm(qr) \right] \\ v_z^\pm(\Lambda, r) &= iq\xi_n^\pm(qr)F^\pm(\Lambda) + iqH^\pm(\Lambda) \left[|q|r\tilde{\xi}_n^\pm(qr) + \xi_n^\pm(qr) \right].\end{aligned}$$

$$\text{where } \tilde{\xi}^+(qr) \equiv \left. \frac{dK_n(u)}{du} \right|_{u=|q|r}, \quad \tilde{\xi}^-(qr) \equiv \left. \frac{dI_n(u)}{du} \right|_{u=|q|r}$$

The 6 unknown coefficients F^\pm, G^\pm, H^\pm can be solved in terms of membrane mode coefficient

A using the following 6 equations derived from the no-slip boundary condition (Eq.(5) of main text):

$$\begin{aligned} v_r^\pm(\Lambda, R) &= 0, & \Lambda^\alpha v_\alpha^\pm(\Lambda, R) &= 0 \\ i\epsilon^{\alpha\gamma}\Lambda_\gamma v_\alpha^\pm(\Lambda, R) &= -\Lambda_\beta\Lambda^\beta A(\Lambda) \end{aligned}$$

The solution for the 6 coefficients F^\pm, G^\pm, H^\pm is next obtained in *Mathematica*. Plugging in these solutions, the required antisymmetric derivative of the traction vector T_α is given as follows:

$$\epsilon^{\alpha\gamma}D_\gamma\sigma_{\alpha r}^\pm|_{r=R} = \eta_\pm \int D\Lambda e^{i\Lambda_\mu x^\mu} \frac{A(\Lambda)}{R^3} C^\pm(\Lambda) \quad (\text{A4})$$

where

$$C^\pm(n, k) = \frac{2n^2 [\rho^\pm(n, k)]^3 + (n^2 + k^2)^2 [\rho^\pm(n, k)]^2 + 2\rho^\pm(n, k) (k^4 - n^4) - (k^2 + n^2)^3}{\rho^\pm(n, k) k^2 - [\rho^\pm(n, k) - n] [\rho^\pm(n, k) + n] [\rho^\pm(n, k) + 2]} \quad (\text{A5})$$

and

$$k \equiv qR. \quad \rho^\pm(n, k) \equiv \frac{|k|\tilde{\xi}_n^\pm(k)}{\xi_n^\pm(k)}. \quad (\text{A6})$$

More explicitly,

$$\rho_+[n, k] = \frac{|k|\frac{dK_n[u]}{du}|_{u=|k|}}{K_n[|k|]}, \quad \rho_-[n, k] = \frac{|k|\frac{dI_n[u]}{du}|_{u=|k|}}{I_n[|k|]} \quad (\text{A7})$$

The fundamental equation of stress balance on the cylindrical membrane (after taking anti-symmetric derivative of both sides of Eq.(2) of main text) thus reads as

$$-\epsilon^{\alpha\beta}D_\beta[\tau \epsilon_{\alpha\gamma}D^\gamma] \underbrace{\left(\frac{1}{4\pi^2 R} \int d\Lambda e^{i\Lambda_\beta(x-x_0)^\beta}\right)}_{\delta^2(\theta-\theta_0, z-z_0)} = \int d\Lambda \frac{\eta_{2D} A(\Lambda)}{R^4} \underbrace{c_n(k)}_{\text{membrane stress} + \text{Traction}} e^{i\Lambda_\alpha x^\alpha}$$

with

$$c_n(k) = (n^2 + k^2)^2 - \frac{R}{\lambda_-} C^-(n, k) + \frac{R}{\lambda_+} C^+(n, k) \quad (\text{A8})$$

We solve for $A(\Lambda)$ from the above equation as

$$A(\Lambda) = \frac{\tau R}{4\pi^2 \eta_{2D}} \frac{n^2 + k^2}{c_n(k)} e^{-i\Lambda_\alpha x^\alpha} \quad (\text{A9})$$

Plugging this solution of $A(\Lambda)$ into Eq.(A3), we get

$$v_\alpha = \epsilon_{\alpha\beta} D^\beta \underbrace{\left(\int d\Lambda \frac{\tau R}{4\pi^2 \eta_{2D}} \frac{n^2 + k^2}{c_n(k)} e^{i\Lambda \cdot (\mathbf{x} - \mathbf{x}_0)} \right)}_{\equiv \psi} \quad (\text{A10})$$

where we can now identify the stream function of the flow field at (θ, z) sourced by a vortex of strength τ situated at the origin

$$\psi(\theta, z) = \frac{\tau}{4\pi^2 \eta_{2d}} \sum_{n=-\infty}^{\infty} \int_{-\infty}^{\infty} dk \frac{n^2 + k^2}{c_n(k)} e^{i(n\theta + \frac{k}{R}z)}. \quad (\text{A11})$$

The vortex flow velocity is given in terms of ψ as

$$\begin{aligned} v_\theta &= \partial_z \psi \\ v_z &= -\frac{1}{R} \partial_\theta \psi \end{aligned} \quad (\text{A12})$$

In the high curvature limit and assuming $\eta_- = \eta_+ \equiv \eta$,

$$\lim_{R/\lambda \rightarrow 0} c_n(k) = \begin{cases} k^4 + 2k^2 \frac{R}{\lambda} & n = 0 \\ (k^2 + n^2)^2 & n \geq 1 \end{cases} \quad (\text{A13})$$

In this limit, we can perform the integrals and sums analytically, leading to the following stream function for a vortex of strength τ located at the origin

$$\psi(\theta, z) = \frac{\tau}{4\pi \eta_{2D}} \left(-\log \left[1 - 2e^{-\frac{|z|}{R}} \cos \theta + e^{-\frac{2|z|}{R}} \right] + \sqrt{\frac{\lambda}{2R}} e^{-\frac{\sqrt{2}|z|}{\sqrt{\lambda R}}} \right) \quad (\text{A14})$$

which is the Eq.(7) of main text.

The corresponding vortex flow at the location (θ, z) sourced by a vortex of strength τ , situated at (θ_0, z_0) is given by

$$\begin{aligned} v_\theta &= \frac{\tau}{4\pi \eta_{2D} |z - z_0|} \left(\frac{2 - 2 \cos(\theta - \theta_0) e^{\frac{|z - z_0|}{R}}}{1 + 2e^{\frac{|z - z_0|}{R}} - 2 \cos(\theta - \theta_0) e^{\frac{|z - z_0|}{R}}} - \frac{e^{-\sqrt{\frac{2}{R\lambda}} |z - z_0|} (z - z_0)}{R} \right) \\ v_z &= -\frac{\tau}{4\pi \eta_{2D} R} \frac{\sin(\theta - \theta_0)}{\cos(\theta - \theta_0) - \cosh \frac{z - z_0}{R}} \end{aligned} \quad (\text{A15})$$

which is Eq.(8) of main text. Note that in the limit $z \rightarrow z_0$, the vortex flow Eq.(A15) simplifies to

$$\begin{aligned} \lim_{z \rightarrow z_0} v_\theta &= 0 \\ \lim_{z \rightarrow z_0} v_z &= \frac{\tau}{4\pi R} \frac{\cot\left(\frac{\theta - \theta_0}{2}\right)}{\eta_{2d}} \end{aligned} \quad (\text{A16})$$

and in the limit $\theta \rightarrow \theta_0$, the vortex flow Eq.(A15) simplifies to

$$\lim_{\theta \rightarrow \theta_0} v_\theta = -\frac{\tau(z-z_0)}{4\pi R \eta_{2D} |z-z_0|} \left(e^{-\sqrt{\frac{2}{R\lambda}}|z-z_0|} + \frac{2}{-1+e^{-\frac{|z-z_0|}{R}}} \right)$$

$$\lim_{\theta \rightarrow \theta_0} v_z = 0 \tag{A17}$$

Appendix B: Contour plots for level sets of the Hamiltonian and helix pitch

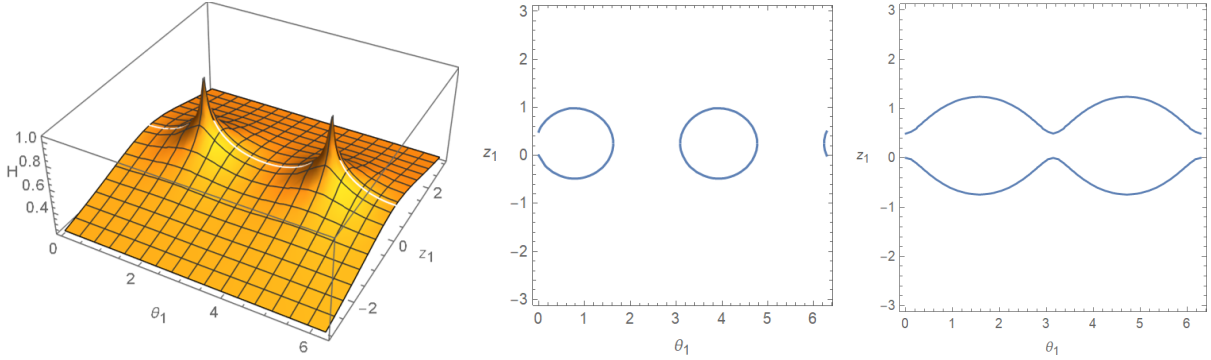


FIG. 9: Left: 3D plot of the Hamiltonian given by Eq. (9) as a function of (θ_1, z_1) , after eliminating the coordinates of the second vortex (θ_2, z_2) using Eq. (12) of main text. Middle: Contour plot of the level set of the Hamiltonian for the initial conditions described in Fig. (2a) and Fig. (2b) The contour plots are closed loops. Right: Contour plot of the level set of the Hamiltonian for the initial conditions of Fig. (2c). They traverse the entire angular direction of the cylinder, consistent with the simulation results of main text.

The time period T for one complete rotation around the membrane tube of radius R for the helical motion in Fig. (2f) for a vortex pair with $\tau_1 = -\tau_2 \equiv \tau$ can be easily constructed from the fact that in this situation $\dot{\theta}_1 = \dot{\theta}_2$ and $\dot{z}_1 = \dot{z}_2$, which implies that the *theta* and *z* separation between the vortices remain constant in time. Thus, we can utilize the velocity expression in Eq. (11) to find the time period T (note that the velocities depend on the separation in θ and z and hence are constants as well)

$$\frac{2\pi R}{T} = \left| \frac{\tau(z_1^i - z_2^i)}{4\pi R \eta_{2D} |z_1^i - z_2^i|} \left(\frac{2 - 2\cos(\theta_1^i - \theta_2^i) e^{-\frac{|z_1^i - z_2^i|}{R}}}{1 + e^{-\frac{|z_1^i - z_2^i|}{R}}} - 2\cos(\theta_1^i - \theta_2^i) e^{-\frac{|z_1^i - z_2^i|}{R}} \right) \right|$$

where (θ_1^i, z_1^i) and (θ_2^i, z_2^i) are the initial vortex locations. Thus, the pitch of the helix Δz

can be computed from the $\dot{z}_1 = \dot{z}_2$ expression in Eq. (11) and is given by

$$\begin{aligned} \Delta z &= \left| T \frac{\tau}{4\pi\eta_2 D R} \frac{\sin(\theta_1^i - \theta_2^i)}{\cos(\theta_1^i - \theta_2^i) - \cosh \frac{z_1^i - z_2^i}{R}} \right| \\ &= \left| \frac{\frac{2\pi R \sin(\theta_1^i - \theta_2^i)}{\cos(\theta_1^i - \theta_2^i) - \cosh \frac{z_1^i - z_2^i}{R}} \frac{|z_1^i - z_2^i|}{(z_1^i - z_2^i)}}{\frac{2 - 2 \cos(\theta_1^i - \theta_2^i)}{1 + e^{-\frac{2|z_1^i - z_2^i|}{R}}} e^{\frac{|z_1^i - z_2^i|}{R}} - e^{-\sqrt{\frac{2}{R\lambda}} |z_1^i - z_2^i|}}{\frac{2|z_1^i - z_2^i|}{R} - 2 \cos(\theta_1^i - \theta_2^i) e^{\frac{|z_1^i - z_2^i|}{R}}}} \right| \end{aligned} \quad (\text{B1})$$

Data Availability The analytical data that support the findings of this study are available within the article and its supplementary material. Numerical details and additional data are available from the authors upon reasonable request.

-
- [1] S. J. Singer and G. L. Nicolson, *The fluid mosaic model of the structure of cell membranes*, Science **175**, 720 (1972)
- [2] E.M. Purcell, *Life at low Reynolds number*, American Journal of Physics 45, 3 (1977)
- [3] P. G. Saffman, *Brownian motion in thin sheets of viscous fluid*, J. Fluid Mech. 73:593–602, (1975)
- [4] P. G. Saffman and M. Delbrück, *Brownian motion in biological membranes*, Proc. Natl. Acad. Sci. USA. 72:3111–3113 (1975)
- [5] B. D. Hughes, B. A. Pailthorpe, and L. R. White, *The translational and rotational drag on a cylinder moving in a membrane*, J. Fluid Mech. **110**, 349–372 (1981)
- [6] E. Evans, and E. Sackmann, *Translational and rotational drag coefficients for a disk moving in a liquid membrane associated with a rigid substrate*, J. Fluid Mech. **194**, 553–561 (1988)
- [7] D.K. Lubensky and R.E. Goldstein, *Hydrodynamics of monolayer domains at the air–water interface*, Physics of Fluids **8**, 843 (1996)
- [8] H. A. Stone, and A. Ajdari. *Hydrodynamics of particles embedded in a flat surfactant layer overlying a subphase of finite depth*, Journal of Fluid Mechanics **369** (1998)
- [9] T.M. Fischer, *The drag on needles moving in a Langmuir monolayer*, J. Fluid. Mech. **498**, 123 (2004)
- [10] A. Naji, A.J. Levine and P.A. Pincus, *Corrections to the Saffman–Delbrück mobility for membrane bound proteins*, Biophysical Journal, **93**, Issue 11, L49–L51 (2007)

- [11] DR Daniels and MS Turner, *Diffusion on membrane tubes: A highly discriminatory test of the Saffman-Delbruck theory*, *Langmuir* **23**:6667–6670 (2007)
- [12] N. Oppenheimer and H. Diamant, *Correlated diffusion of membrane proteins and their effect on membrane viscosity*, *Biophysical Journal* **96**, 3041–3049 (2009).
- [13] N. Oppenheimer and H. Diamant *Correlated dynamics of inclusions in a supported membrane*, *Physical Review E* **82**, 041912 (2010).
- [14] N. Oppenheimer and H. Diamant, *Dynamics of membranes with immobile inclusions*, *Physical Review Letters* **107**, 258102 (2011).
- [15] M. L. Henle, R. McGorty, A. B. Schofield, A. D. Dinsmore, A. J. Levine, *The effect of curvature and topology on membrane hydrodynamics*, *EPL (Europhysics Letters)*, **84**, 48001 (2008)
- [16] M. L. Henle, A. J. Levine, *Hydrodynamics in curved membranes: The effect of geometry on particulate mobility*, *Physical Review E*, **81**, 011905 (2010)
- [17] YA Domanov, S Aimon, GES Toombes, M Renner, F Quemeneur, A Triller, MS Turner, P Bassereau, *Mobility in geometrically confined membranes*, *PNAS* **108** (31):12605 (2011)
- [18] F. G. Woodhouse and R. E. Goldstein, *Shear-Driven Circulation Patterns in Lipid Membrane Vesicles*, *J. Fluid Mech.* **705**, 165 (2012)
- [19] A. R. H. Smith, F. G. Woodhouse, V. Kantsler, R. E. Goldstein, *Membrane Viscosity Determined from Shear-Driven Flow in Giant Vesicles*, *PRL* **111**, 038103 (2013)
- [20] F. Quemeneura, J. K. Sigurdsson, M. Rennerf, P. J. Atzberger, P. Bassereaua, and D. Lacoste, *Shape matters in protein mobility within membranes*, *Proceedings of the National Academy of Sciences (PNAS)*, **11**, No. 14, pg. 5083–5087, (2014)
- [21] D.R. Daniels, *Curvature correction to the mobility of fluid membrane inclusions*, *The European Physical Journal E*, **39**, 96 (2016)
- [22] J. K. Sigurdsson and P. J. Atzberger, *Hydrodynamic Coupling of Particle Inclusions Embedded in Curved Lipid Bilayer Membranes*, **12**, 6685-6707, *Soft Matter*, The Royal Society of Chemistry, (2016)
- [23] B. J. Gross and P. J. Atzberger, *Hydrodynamic Flows on Curved Surfaces : Spectral Numerical Methods for radial manifold shapes*, *Journal of Computational Physics*, **371**, 663 (2018)
- [24] A Sahu, Y.A.D. Omar, R.A. Sauer and K.K. Mandadapu, *Arbitrary Lagrangian–Eulerian finite element method for curved and deforming surfaces I. General theory and application to fluid interfaces*, *Journal of Computational Physics* **407**, 109253 (2020)

- [25] D. Rower, M. Padidar and P. J. Atzberger, *Surface Fluctuating Hydrodynamics methods for the drift-diffusion dynamics of particles and microstructures within curved fluid interfaces*, Journal of Computational Physics **455**, 110994
- [26] R. Samanta and N. Oppenheimer, *Vortex Flows and Streamline Topology in Curved Biological Membranes*, Physics of Fluids **33**, 051906 (2021)
- [27] P.D.Tran, T.A.Blanpied and P.J. Atzberger, *Protein drift-diffusion dynamics and phase separation in curved cell membranes and dendritic spines: Hybrid discrete-continuum methods*, Physical Review E **106**, 044402 (2022)
- [28] S. Bagaria and R. Samanta *Dynamics of force dipoles in curved fluid membranes*, Phys. Rev. Fluids **7**, 093101 (2022)
- [29] S. Jain and R. Samanta, *Force dipole interactions in tubular fluid membranes*, Physics of Fluids **35**, 071901 (2023)
- [30] W Shi, M Moradi, and E Nazockdast, *Hydrodynamics of a single filament moving in a spherical membrane*, Phys. Rev. Fluids **7**, 084004 (2022)
- [31] E. Climent, K. Yeo, M. Maxey, GE Karniadakis, *Dynamic self-assembly of spinning particles*, J. Fluids Eng. **129**(4), 379–387 (2007)
- [32] D. Das, D. Saintillan, *Electrohydrodynamic interaction of spherical particles under Quincke rotation*, Phys. Rev. E **87**, 043014 (2013)
- [33] Y. Fily, A. Baskaran, M.C. Marchetti, *Cooperative self-propulsion of active and passive rotors*. SoftMatter **8**, 3002–3009 (2012)
- [34] M.E.J. Friese, T.A. Nieminen, , N.R. Heckenberg, H. Rubinsztein-Dunlop, *Optical alignment and spinning of laser-trapped microscopic particles*, Nature **394**, 348–350 (1998)
- [35] S. Fürthauer, M. Stempel, S.W. Grill, F. Jülicher, *Active chiral processes in thin films*, Phys. Rev. Lett. **110**, 048103 (2013)
- [36] B.S. Grzybowski, H.A. Stone, G.M. Whitesides, *Dynamic self-assembly of magnetized, millimetre-sized objects rotating at a liquid air interface*, Nature **405**, 1033–1036 (2000)
- [37] B.A. Grzybowski, X. Jiang, H.A. Stone, G.M. Whitesides, *Dynamic, self-assembled aggregates of magnetized, millimeter-sized objects rotating at the liquid–air interface*, Phys. Rev. E **64**, 011603 (2001)
- [38] B.A. Grzybowski, G.M. Whitesides, *Dynamic aggregation of chiral spinners*. Science *296*, 718–721 (2002)

- [39] M. Leoni, T.B. Liverpool: *Dynamics and interactions of active rotors*, Europhys. Lett. *92*, 64004 (2010)
- [40] I. Llopis, I. Pagonabarraga: *Hydrodynamic regimes of active rotators at fluid interfaces*, Eur. Phys. J. E **26**, 103–113 (2008)
- [41] E. Lushi and P. M. Vlahovska, *Periodic and Chaotic Orbits of Plane-Confined Micro-rotors in Creeping Flows*, J. Nonlinear Sci. *25*, 1111 (2015)
- [42] K. Yeo, E. Lushi, and P. M. Vlahovska, *Collective Dynamics in a Binary Mixture of Hydrodynamically Coupled Microrotors*, Phys. Rev. Lett. *114*, 188301 (2015)
- [43] A. Modin, M.Y.B. Zion and P.M. Chaikin, *Hydrodynamic spin-orbit coupling in asynchronous optically driven micro-rotors*, Nature Communications **14**, Article number: 4114 (2023).
- [44] P. Lenz, J.F. Joanny, F. Jülicher and J. Prost, *Membranes with Rotating Motors*, Phys. Rev. Lett **91**, 108104 (2003)
- [45] P. Lenz, J.F. Joanny, F. Jülicher and J. Prost, *Membranes with rotating motors: Microvortex assemblies*, Eur. Phys. J. E **13**, 379 (2004)
- [46] N. Oppenheimer, D. B. Stein and M. J. Shelley, *Rotating membrane inclusions crystallize through hydrodynamic and steric interactions*, Phys. Rev. Lett. *123*, 148101 (2019)
- [47] N. Oppenheimer, D. B. Stein, M. Y. B. Zion, and M. J. Shelley, *Hyperuniformity and phase enrichment in vortex and rotor assemblies*, Nature communications **13**, 1 (2022)
- [48] Y. Shoham and N. Oppenheimer, *Hamiltonian Dynamics and Structural States of Two-Dimensional Active Particles*, PRL **131**,178301 (2023)
- [49] Q. Le Thien, D. McDermott, C.J.O. Reichhardt, and C. Reichhardt, "Enhanced pinning for vortices in hyperuniform substrates and emergent hyperuniform vortex states," Phys. Rev. B **96**, 094516 (2017)
- [50] Y. Kimura, *Vortex Motion on Surfaces with Constant Curvature*, Proceedings: Mathematical, Physical and Engineering Sciences, **455**,1981, page 245–259 (1999)
- [51] J. Montaldi, A. Soulière and T. Tokieda, *Vortex Dynamics on a Cylinder*, SIAM J. Appl. Dyn. Syst., **2**, no. 3, pp. 417–430 (2003)
- [52] J. Andrade, S. Boatto, T. Combrot, G. Duarte and T.J. Stuchi, *N-body Dynamics on an Infinite Cylinder: the Topological Signature in the Dynamics*, Regular and Chaotic Dynamics, **25**, No.1, pp.78–110 (2020)
- [53] Y. Sokolov and H. Diamant, *Many-particle mobility and diffusion tensors for objects in viscous*

- sheets*, J. Chem. Phys. **149**, 034901 (2018)
- [54] J. Happel and H. Brenner, *Low Reynolds Number Hydrodynamics with Special Applications to Particulate Media*, Kluwer, The Netherlands (1983)
- [55] Wolfram Research, Inc., Mathematica, Champaign, IL.